Biol. Cybern. 70, 209–217 (1994)

Biological Cybernetics

A nonstationary Poisson point process describes the sequence of action potentials over long time scales in lateral-superior-olive auditory neurons

Robert G. Turcott [1], Steven B. Lowen [1], Eric Li [1], Don H. Johnson [2], Chiyeko Tsuchitani [3], Malvin C. Teich [4]

[1] Department of Electrical Engineering, Columbia University, New York, NY 10027, USA
[2] Department of Electrical and Computer Engineering, Rice University, Houston, TX 77251, USA
[3] Sensory Science Center, University of Texas Health Science Center, Houston, TX 77030, USA
[4] Departments of Electrical Engineering and Applied Physics, Columbia University, New York, NY 10027, USA

Received: 15 January 1993/Accepted in revised form: 21 June 1993

Abstract. The behavior of lateral-superior-olive (LSO) auditory neurons over large time scales was investigated. Of particular interest was the determination as to whether LSO neurons exhibit the same type of fractal behavior as that observed in primary VIII-nerve auditory neurons. It has been suggested that this fractal behavior, apparent on long time scales, may play a role in optimally coding natural sounds. We found that a nonfractal model, the nonstationary dead-time-modified Poisson point process (DTMP), describes the LSO firing patterns well for time scales greater than a few tens of milliseconds, a region where the specific details of refractoriness are unimportant. The rate is given by the sum of two decaying exponential functions. The process is completely specified by the initial values and time constants of the two exponentials and by the dead-time relation. Specific measures of the firing patterns investigated were the interspike-interval (ISI) histogram, the Fano-factor time curve (FFC), and the serial count correlation coefficient (SCC) with the number of action potentials in successive counting times serving as the random variable. For all the data sets we examined, the latter portion of the recording was well approximated by a single exponential rate function since the initial exponential portion rapidly decreases to a negligible value. Analytical expressions available for the statistics of a DTMP with a single exponential rate function can therefore be used for this portion of the data. Good agreement was obtained among the analytical results, the computer simulation, and the experimental data on time scales where the details of refractoriness are insignificant. For counting times that are sufficiently large, yet much smaller than the largest time constant in the rate function, the Fano factor is directly proportional to the counting time. The nonstationarity may thus mask fractal fluctuations, for which the Fano factor increases as a fractional power (less than unity) of the counting time.

Correspondence to: M. C. Teich

1 Introduction

The sequence of action potentials propagating down the axon of a neuron can be mathematically modeled as a point process in which the action potentials are viewed as points on the time axis. Point processes are characterized in terms of a counting process, which is a record of the number of points $N_T(t)$ in the counting interval $(t, t + T]$, or in terms of a sequence of interevent times τ_i between points $i - 1$ and i (Cox and Lewis 1966; Teich and Khanna 1985).

Extensive work has been carried out in investigating the short time properties of lateral-superior-olive (LSO) neural firing patterns, such as refractoriness and chopper activity (Tsuchitani and Johnson 1985; Johnson et al. 1986).

In this paper, we specifically address the long time behavior of the stream of neural impulses in LSO units. To our knowledge, this behavior has not been previously investigated. VIII-nerve units exhibit fractal behavior; the sequence of action potentials, for both spontaneous and pure-tone stimuli, is well modeled by a stationary point process with fractional power-law correlation (Teich 1989, 1992; Teich et al. 1990a, b). Since naturally occurring sounds exhibit this same kind of correlation, the fractal aspect of the VIII-nerve firing patterns may play a role in the optimal sampling of sound (Teich 1989). One of the principal purposes of this study was to determine whether LSO units exhibit the same type of a long-duration fractal behavior as do VIII-nerve units. We found, however, that a nonfractal, nonstationary point-process model is adequate for describing the long time scale statistics of the firing patterns of the LSO units we investigated.

After discussion of the experimental methods and results, the model is presented in Sect. 4. The results predicted by the model are compared with the experimental results in Sect. 5, and the salient points are summarized in Sect. 6. The derivation of analytical results is presented in the Appendix.

2 Methods

2.1 Experimental arrangement

The LSO nucleus is one of the first stations in the ascending auditory pathway directly involved in processing binaural signals. It is one of the three main nuclei of the cat's superior olivary complex involved in the processing of interaural cues used in binaural perceptual tasks. While all LSO units are excited by stimulation of the ipsilateral ear, in the cat the ipsilaterally elicited discharges of those LSO units with characteristic frequencies (CFs, to which the unit is most sensitive) above 1 kHz can also be inhibited by simultaneous stimulation of the contralateral ear (Tsuchitani and Boudreau 1966; Guinan et al. 1972). Consequently, the LSO units most sensitive to mid- to high-frequency signals are capable of encoding the interaural level difference created by the sound shadowing effects of the head and pinna to shorter wavelength stimuli. The ipsilateral excitatory input is supplied by neurons in the anteroventral cochlear nucleus (Cant and Casseday 1986), and the contralateral inhibitory input by neurons in the medial nucleus of the trapezoid body (Zook and DiCaprio 1988). The discharge statistics of LSO unit discharges to monaural and binaural tone bursts have been described elsewhere (Tsuchitani 1982; Johnson et al. 1986; Zacksenhouse et al. 1993).

In the experiments reported here, single-unit discharges were recorded from units histologically localized in the LSO of barbiturate-anesthetized cats. Long-duration tones set to ipsilateral CF were delivered monaurally at 25–30 dB above unit CF threshold. Details of the preparation and experiment, and a number of short time scale statistical measures, have been described elsewhere (Tsuchitani and Johnson 1985; Tsuchitani 1988).

2.2 Statistical measures

Several well-known statistical measures that are valid over a wide range of time scales are used in the analysis of the data presented here and are briefly described.

The interspike-interval (ISI) probability density function completely describes the behavior of the point process only if the interevent times are independent and identically distributed random variables, in which case the process is called a renewal point process. The ISI histogram is an estimate of this function from a finite set of data. When the interevent times are not independent of each other, the ISI still yields information about the process over short time scales, but it fails to provide information about the behavior of the process over longer time scales (i.e., times much greater than the average interevent time). This is clearly true for data such as those examined here, where the rate varies. It also holds for data with a constant average rate, but with correlation among the events.

The Fano-factor time curve (FFC) and the serial count correlation coefficient (SCC) time curve complement the ISI by providing information about the process over longer time scales (Teich 1989; Teich et al. 1990a, b; Teich 1992). The Fano factor for a given counting time T is the ratio of the variance to the mean of the number of counts in that counting time. The homogeneous Poisson point process (HPP) is a ubiquitous mathematical model; it plays the role in point process theory that Gaussian noise plays in the theory of continuous stochastic processes (Saleh and Teich 1982). For the HPP the variance is equal to the mean for all counting times, giving a Fano factor of unity (see Sect. 4.1). The FFC therefore provides a convenient comparison between an arbitrary point process and the HPP. A Fano factor less than unity indicates that the process has more regularity than the HPP at that particular counting time; the statistics are then said to be sub-Poisson. Dead time (refractoriness) typically imposes such regularity on a point process. A Fano factor greater than unity indicates more variability than the HPP at that particular counting time, as observed with a nonstationary Poisson point process (e.g., the model presented in this paper) or with an inhomogeneous, stationary Poisson point process (e.g., the fractal shot-noise-driven Poisson point process, which has a stochastically varying rate, but whose statistics are independent of time; see Teich et al. 1990a, b; Lowen and Teich 1991). Aside from the magnitude of the Fano factor at a particular counting time, the functional dependence of the Fano factor on the counting time gives further information about the process, such as the form of the temporal correlation (Teich 1989). In particular, for many inhomogeneous Poisson point processes with deterministic rate functions, the FFC is directly proportional to the counting time T for a certain range of T (Teich and Diament 1969; Prucnal and Teich 1979).

The SCC is an estimate of the correlation between the number of events in successive counting intervals and is calculated as a function of the counting time. An SCC of zero implies that the number of events in successive intervals are uncorrelated. A negative SCC indicates that the number is negatively correlated, so that an above-average count in one interval is usually preceded or followed by a below average count in the adjacent intervals. This type of behavior is typically observed when the counting time is on the order of the dead time. Conversely, positive correlation is indicated by a positive SCC. The closer the SCC approaches ± 1, the more strongly the counting process is positively or negatively correlated. The SCC and the FFC are related since both are obtained from the first and second moments of the counting process. It can be shown that for a process whose FFC has a fractional power-law dependence on the counting time, i.e., FFC $\propto T^{\alpha}$, $\alpha \in [0, 1)$, the SCC is constant and equal to $2^{\alpha} - 1$ (Cox and Lewis 1966; Teich et al. 1990b). A typical nonstationary Poisson process with a deterministic rate function yields α close to unity; for sufficiently large T we then expect FFC $\propto T$ and SCC ≈ 1.

Since all joint statistics are necessary to define uniquely a stochastic process, the ISI histogram, the FFC, and SCC, being first- and second-order measures, do not provide complete information about the process. Nevertheless, when used in conjunction they are useful for providing a basic characterization of the process on all time scales.

3 Results

The average intensity (firing rate) as a function of time, ISI histogram, FFC, and SCC were estimated from five long-duration recordings from the three LSO units. Two of these were fast-chopper cells, and one was a slow-chopper cell. All had unimodal ISI histograms. In Figs. 1–4 we present these four measures from a single recording (t176–IE.r2, denoted r2 for brevity); these curves are representative of the statistical measures estimated from the recordings we examined. The duration of the recording for this particular data set was approximately 555 s.

Figure 1 shows an estimate of the average intensity obtained by recording the number of action potentials that fall in successive 1-s counting intervals. After the onset of the stimulus the rate falls quickly to about 100 s^{-1}, then decays more slowly over the remainder of the recording. The rapid fluctuations in the rate estimate result from the randomness inherent in the spike train.

The ISI histogram was estimated from the entire duration of the recording. It is presented in Fig. 2a, where the solid curve corresponds to the data. The effect of refractoriness is apparent in the reduced probability of short intervals. The approximately straight-line behavior of the data for interevent times greater than 10 ms, on this semilogarithmic plot, suggests that the intervals are exponentially distributed, which would be consistent with an HPP. However, the time-varying rate function shown in Fig. 1 clearly indicates that the process is in fact *not* homogeneous.

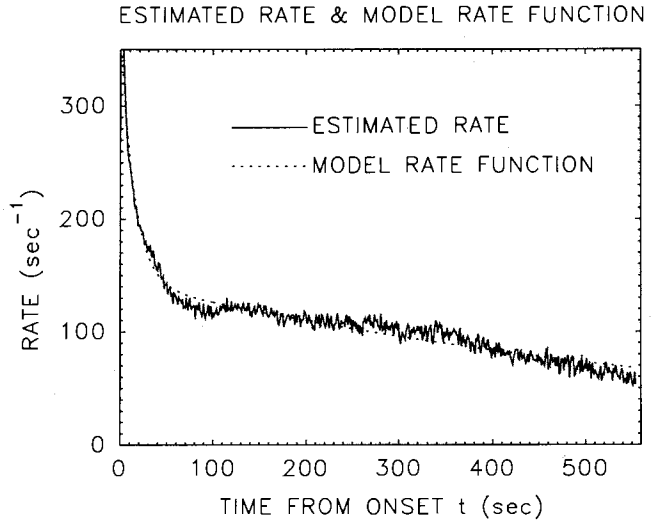

Fig. 1. The average intensity $\lambda_d(t)$ as a function of time from the onset of the recording estimated from unit r2 (*solid curve*) and the exponentially decaying model rate function obtained from the best-fitting parameters presented in Table 1 (*dotted curve*). The rate functions of the lateral-superior-olive (LSO) units were obtained by counting the number of action potentials that fell in successive 1.0-s intervals using the entire duration of the recording. The results for this unit are typical of those examined. The first few seconds of the data were ignored in obtaining the best-fitting rate parameters because the recording was initiated slightly before the stimulus was applied

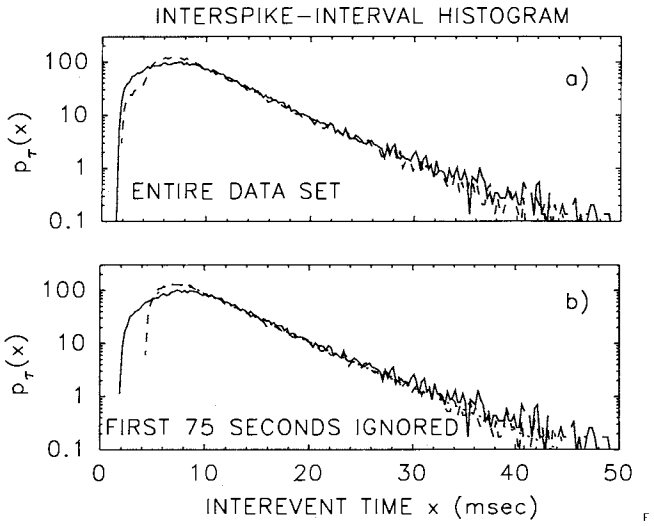

Fig. 2. a Interval density functions (ISI histograms) $p_\tau(x)$ estimated from the entire data set of unit r2 (*solid curve*) and from a simulated spike train (*dashed curve*) of the same duration, using the model developed in Sect. 4, with the best fitting parameters shown in Table 1. **b** The interspike interval (ISI) histograms obtained with the first 75 s of data ignored. Also shown, but partially obscured by the *dashed curve*, is the analytical ISI probability density function derived in the Appendix (*dotted*). The straight-line appearance on this semilogarithmic plot for interevent times greater than 10 ms is consistent with the ISI histogram of a homogeneous Poisson process, but this process is clearly inhomogeneous. This illustrates the danger of drawing conclusions about a point process based solely on the ISI histogram

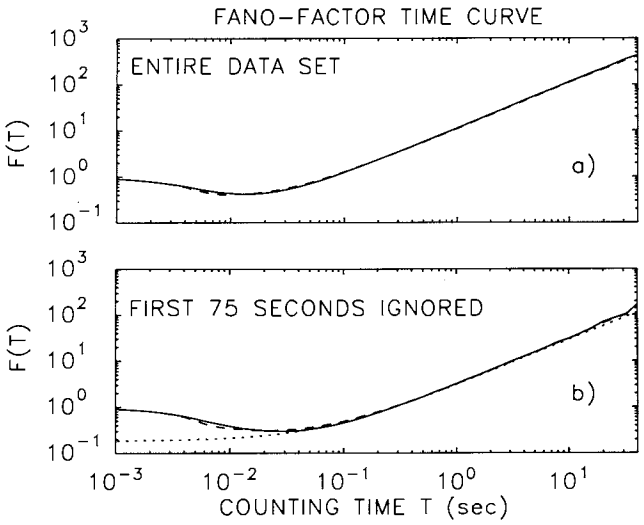

Fig. 3a, b. Fano-factor time curves (FFCs) obtained from the same spike trains that were used to generate the ISI histograms in Fig. 2 (unit r2). **a** The FFC for the data (*solid*) and the simulation (*dashed*) were generated from the entire data set. **b** The results obtained from the truncated data and simulated spike trains, along with the analytical results. For large counting times the Fano factor is proportional to the counting time T, as is typical for an inhomogeneous Poisson process with a deterministic rate function. The dip of the FFC below unity in the vicinity of 20 ms reflects regularity in the spike train imposed by refractoriness. At larger counting times, this regularity is overwhelmed by excess variance introduced by the correlation present at these time scales. This correlation is a result of the deterministic rate function. The analytical results (*dotted*) agree with the data (*solid*) and simulation (*dashed*) for $T \gg \tau_d$ (which was assumed to hold in the analytical derivation), where τ_d is the dead time or refractory period

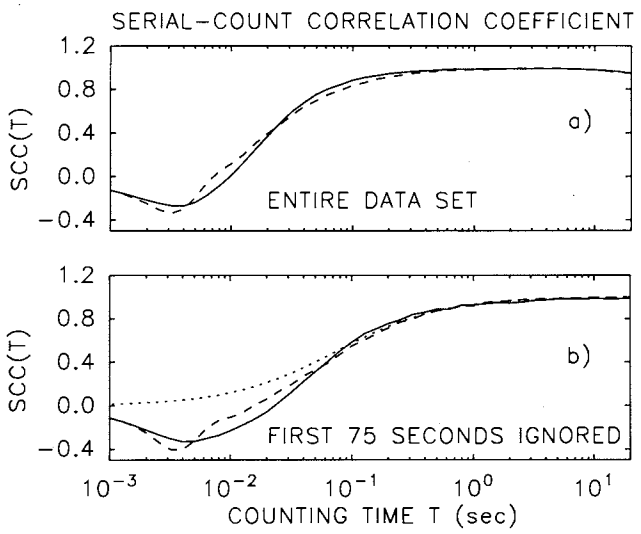

Fig. 4a, b. Serial count-correlation coefficient curves (SCCs) obtained from the same spike trains that provided the other statistical measures (unit r2). **a** The entire recording was used to generate the SCC for the data (*solid*) and simulation (*dashed*). **b** The analytical results are presented (*dotted*), along with the results from the truncated spike trains. Refractoriness imposes a depression in the correlation for counting times less than approximately 10 ms. Since the analytical results do not include the effects of dead time, they do not predict the negative correlation apparent in the data and simulation. For longer time scales, the positive correlation imposed by the deterministic rate function is apparent. The results for the data and simulation differ slightly at intermediate time scales because of the simple way in which the dead time was modeled. At longer time scales, the data, simulation, and analytical curves all converge to unity as predicted by the theory

The FFC for this unit is presented in Fig. 3a (solid curve). The regularity imposed by refractoriness results in a variance-to-mean ratio (Fano factor) less than unity for counting times less than about 40 ms. The increase in the Fano factor for large counting time suggests that there is correlation in the spike train. The decaying rate function is the likely source of this correlation.

The SCC is shown in Fig. 4a, where again the solid curve corresponds to the data. The negative correlation imposed by refractoriness is evident at short time scales. For counting times greater than about 100 ms, the SCC, like the FFC, indicates that long-term correlation is present, overwhelming the negative correlation imparted by refractoriness.

4 Theory

4.1 Background

The Poisson point process is a memoryless point process whose interevent times are determined by a single parameter $\lambda(t)$, which is associated with the density of points. The well-known homogeneous (constant-rate) Poisson process (HPP) gives rise to a sequence of independent, identically distributed (exponential) random variables corresponding to the intervals between adjacent points on the time axis. For the HPP, $\lambda(t)$ is a constant, λ. The process is renewal since all interevent times are independently generated from the same probability density function. The number of points in nonoverlapping counting intervals are independent, so that the joint statistics of the interevent times, as well as the numbers of counts in nonoverlapping counting intervals, are determined solely by their marginal statistics. The marginal count distribution is Poisson with parameter $M_T = \lambda T$.

The nonstationary Poisson process is a Poisson point process whose rate has statistics that vary time. In contrast, the doubly stochastic Poisson point process (DSPP) is a stationary Poisson process with a rate (intensity) function that varies stochastically, but whose statistics are constant with time (Saleh 1978). For example, the rate runction for a DSPP will have a constant expected value. We focus on a particular kind of nonstationary Poisson point process, one with a deterministic time-varying rate $\lambda(t)$. Since the generation of events is memoryless, the value of any interevent time depends only on the time course of the rate function following the previous event. This property allows the statistics of the interevent times to be obtained, conditioned on the occurrence of an event at an arbitrary time t_0. It also allows the joint count statistics of nonoverlapping counting periods to be specified in terms of the marginal distributions. The marginal distribution of counts in the interval $(t, t + T]$ is still Poisson, but with the parameter given by the integrated rate $M_T(t)$ (Saleh 1978):

$$M_T(t) = \int_t^{t+T} \lambda(x)\,dx \tag{1}$$

The linearity of (1) implies that the superposition (sum) of point processes generated from different rate functions is equivalent to the point process generated from the sum of the rate functions. The point processes described so far lend themselves to relatively straightforward analysis because they are both memoryless and linear in the sense described above. Dead time introduces both memory and a nonlinear element, however, so the statistics of a process with dead time are in general difficult to obtain. The homogeneous dead-time-modified Poisson point process (DTMP) exhibits independent, identically distributed (truncated exponential) interevent times, but the dead time imposes negative correlation among the numbers of events in closely spaced nonoverlapping counting intervals. For this process, the effect of dead time τ_d reduces the rate parameter from its original value λ (the rate without dead time) to a new value (Teich 1985) given by

$$\lambda_d = \frac{\lambda}{1 + \tau_d \lambda} \tag{2}$$

The quantity λ can be thought of as the instantaneous intensity of the process if it is set to zero for τ_d seconds after the occurrence of an impulse. The marginal counting distribution is no longer Poisson, but the counts in nonoverlapping intervals are nearly independent when the separation of the intervals is greater than the dead time. As with the HPP, the renewal nature of the DTMP process allows the joint interval distributions to be expressed entirely in terms of the marginal distribution.

Table 1. Summary of data sets examined

Data set		r_1 (s^{-1})	τ_1 (s)	r_2 (s^{-1})	τ_2 (s)	Duration (s)	k
Fast chopper	t176-IE.r2	170.0	14.5	143.4	734.8	555	1.75
	t187-2A.r3	72.5	16.1	69.5	383.0	450	2.25
	t187-2A.r4	53.6	13.9	87.8	315.6	325	2.0
	t187-2A.r5	69.2	15.6	82.1	274.6	125	1.75
Slow chopper	t162-1A.r10	44.75	10.9	105.6	780.2	553	1.5

The values of r_1, τ_1, r_2, and τ_2 were obtained by fitting (3) to an estimate of the data rate function, which was generated by counting the number of impulses in successive 1-s counting times. The value of k was that which provided the best overall agreement between the data and model for the statistical measures used. The coefficients r_1 and r_2 were normalized so that the time origin corresponds approximately to the point when the stimulus was applied. Data prior to this point were ignored in finding the best-fitting parameters

The nonstationary DTMP is more complex. Nevertheless, the interspike-interval statistics, conditioned on the occurrence of an event at time t_0, are determined solely by the time course of the rate function and the nature of the dead time. The behavior of the process prior to t_0 has no bearing on these conditional statistics. This property makes analytical treatment easier and simulation straightforward.

4.2 Model

The average firing rates of the processes recorded from the LSO units examined are well approximated by a function of the form

$$\lambda_d(t) = r_1 \exp(-t/\tau_1) + r_2 \exp(-t/\tau_2) \tag{3}$$

where t is the time since the onset of the recording. Since the stimulus was applied after data acquisition was initiated, the first few seconds of data are ignored in fitting the parameters and in obtaining statistical measures. Figure 1 presents a comparison of the estimated rate function and (3), using the best-fitting parameters presented in Table 1 (the duration of the data set is also shown in the table). The exponential with the smaller time constant dominates the rate function at the onset of the recording, but its effect decreases rapidly, so that for approximately 80% of the recording the rate essentially comprises a single exponential function.

The DTMP has been successfully employed in modeling auditory neural firing patterns over short time scales (Teich and Khanna 1985; Young and Barta 1986). That the LSO firings exhibit refractoriness is apparent from the ISI histogram, which shows a low probability of short (less than a few milliseconds) interevent times; the FFC, which shows a variance-to-mean ratio less than unity on these time scales; and the negative correlation apparent in the SCC time curve for these counting times. These characteristics are all consistent with the presence of refractoriness. The data exhibit shorter dead time at the onset of the recording, when the rate is high, than later, when the rate is low (compare Fig. 2a and b); a similar effect has been noted by Tsuchitani and Johnson (1985). This precludes the use of a simple fixed-dead-time model. As a better approximation, the value of the dead time was taken to be inversely proportional to the rate with dead time, i.e.,

$$\tau_d = \frac{1}{k\lambda_d(t)} \tag{4}$$

Extensive work has been carried out in modeling refractoriness in neural firing patterns (Teich et al. 1978; Teich and Diament 1980; Johnson and Swami 1983; Prucnal and Teich 1983; Teich 1985; Young and Barta 1986; Johnson et al. 1986). We choose the simple form of (4) for dead time because it is analytically tractable, and our focus is on the behavior of the spike train on time scales greater than a few tens of milliseconds, a regime where the particular details of dead time are of diminishing significance. It is preferable not to ignore dead time altogether, however, since it influences the magnitude of the count variance even on large time scales. For these reasons we employ this simple treatment which accounts for the average effect of dead time while allowing the derivation of analytical expressions for various statistical measures to proceed in a straightforward manner.

A single constant of proportionality $1/k$ was obtained for each data set by selecting the value that provided the best overall agreement between the statistical measures (ISI histogram, FFC, SCC) of the data and the model. These values are presented in Table 1.

Analytical expressions for this model, subject to certain restrictions, are derived in the Appendix. We also have performed a computer simulation of the model. Because of the essential Poisson nature of the process, each interevent time depends only on the time course of the instantaneous rate since the expiration of the dead time of the previous spike (Saleh 1978). A nonconstant rate during ISIs can be simulated; however, in the LSO data, there is a high probability that the interevent times are small relative to the time constants of the rate. Therefore the rate can be taken to be constant during the duration of the interval, so the simulation is a straightforward transformation of uniform random variables.

5 Discussion

A comparison of the model rate function in (3) and the estimate from the data is shown in Fig. 1. The model rate function (dotted) describes the estimate from the

data (solid curve) quite well, diverging from the estimate slightly after the decay of the first exponential (around 100 s) and again at the end of the recording.

The ISI histogram, FFC, and SCC were obtained from the data, and from the simulation of the model, using the entire duration of the recording. These measures were also obtained by ignoring the first 75 s in the data and simulation, so that the exponential with the shorter time constant had decayed to a negligible value. In this case we can also compare the analytical results for a single exponential with those of the simulation and the data. All of the data analyses make use of the same spike train.

The ISI histograms using the entire duration of the experiment are presented in Fig. 2a. Results from the data are shown as solid curves, while those from the simulation are dashed. The model describes the data quite well over three decades of probability. The ISI histograms shown in Fig. 2b were obtained with the first 75 s of data ignored. The dotted curve, which is very similar to, and therefore partially hidden by, the dashed curve, corresponds to the analytical formulas derived in the Appendix. The model and data differ most significantly for interevent times in the vicinity of 5 ms. Comparison of the ISI histograms for the experimental data in Fig. 2a and b clearly indicates that our model overestimates the dead time when the rate is low. This is to be expected since a large absolute refractoriness is necessary to model a smaller dead-time region followed by a region of relative refractoriness. Additionally, results obtained using the entire duration of the simulation (Fig. 2a) show a slight dip in the simulated-data histogram (dashed curve) near 2 ms. This irregularity occurs because only the early portion of the entire simulation can generate those interevent times which fall between $\tau_{d,\min}$ and $\tau_{d,\max}$ [see (4) and (A15)]. For the estimates from the truncated data (lacking the first 75 s), the change in rate is small so that $\tau_{d,\min} \approx \tau_{d,\max}$, and the change in τ_d does not produce a significant dip in the curve.

Since our focus is on the long-term behavior of the process, we have used a simple model for dead time. One refinement that improves the fit on short time scales is a modification of the dead-time model such as that used by Young and Barta (1986), which has a random component (specifically, we also used an exponential random variable, but one whose expected value is inversely proportional to the rate) and an absolute component (consisting of a fixed portion and a portion that is inversely proportional to the rate). Johnson et al. (1986) present a higher-order (nonrenewal) model of dead time that accounts for negative serial correlation between successive intervals. These more complex treatments of dead time are useful for understanding the short-term behavior of the spike train. However, they add little understanding to the long-time behavior of the LSO activity, which is our focus, and impose substantial complexity on the model.

Figure 3b shows the FFCs obtained from the data (solid), simulation (dashd), and analytical results (dotted). As with the ISI histogram, the model describes the data quite well. Of particular significance is the agreement over long time scales ($T > 0.1$ s) where the ISI fails to give any meaningful information about the process (see discussion of the ISI histogram in Sect. 2.2). The analytical result converges to the data and simulation when the counting time T becomes much larger than the dead time τ_d, as should be the case because of the assumption $T \gg \tau_d$ used in the derivation. The Fano factor is approximately proportional to the counting time, i.e., $F(T) \propto T^1$.

The SCCs are presented in Fig. 4. Again, the model and data only differ markedly in the region where the role of dead time is significant. The constant correlation indicated by the SCC for large counting times is consistent with the power-law behavior of the FFC. Furthermore, the actual value of the SCC for T sufficiently large tends to unity in agreement with the theory. The derivation of the analytical results neglected the effects of dead time; consequently, the analytical curve in Fig. 4b (dotted) does not show the negative correlation imposed by dead time.

6 Conclusion

The comparison of data, simulation, and analytical results indicates that the inhomogeneous DTMP describes the LSO recordings well, particularly over all time scales longer than 10 ms. Closer agreement with the data on short time scales could be obtained by refining the dead time rule, as indicated in the previous section.

As illustrated by the results, the ISI is useful for describing the short-term characteristics of the process. Indeed, the straight-line form (on semilogarithmic plots) of the ISI histograms shown in Fig. 2 are indistinguishable from those of an HPP. The FFC and SCC capture the long-term behavior of the process; both reflect the correlation imposed by the deterministic rate function. The results suggest that correlation in the data extends beyond the largest observable time scales in our recordings.

Of particular interest is whether the LSO firings exhibit the kind of fractal patterns that are apparent in VIII-nerve fiber recordings (Teich 1989, 1992; Teich et al. 1990a, b). A number of analysis procedures were used in an attempt to separate deterministic, nonstationary rate fluctuations from possible fractal fluctuations. These included Fourier- and wavelet-transform methods, rate normalization, and a quantitative measure of rate fluctuation as a function of counting time. None of these revealed a significant difference between the LSO data and a simulated nonstationary, nonfractal Poisson process. Although the results obtained from the statistical measures described above indicate that a nonfractal, nonstationary Poisson point process models the LSO firings well, it is possible that an underlying fractal component is masked in these measures.

Acknowledgements. This work was supported by the Office of Naval Research under grant N00014-92-J-1251, the National Science Foundation through the Columbia Center for Telecommunications Research, and the National Institutes of Health under grant MH46453.

Appendix
Derivation of the ISI histogram, FFC, and SCC

To obtain expressions for the unmodified rate parameter $\lambda(t)$ in terms of the rate with deal time $\lambda_d(t)$, we use the fact that the rate varies slowly over the duration of typical ISIs. Specifically, since the average interevent time $\langle\tau\rangle$ is small relative to the rate time constants [i.e., $\langle\tau\rangle \ll \tau_1, \tau_2$ in (3)], the rate is approximately constant over an ISI, and we can combine (4) and (2) to obtain

$$\lambda(t) = \frac{k}{k-1}\lambda_d(t) \tag{A1}$$

so that both λ and λ_d are given by the sum of two decaying exponentials.

An analytical expression for the ISI is readily obtained in the case when $\lambda(t)$ is a single exponential

$$\lambda(t) = \lambda_1 \exp(-t/\tau_1) \tag{A2}$$

We define the conditional distribution function $F_\tau(x\,|\,t_0)$ of the interevent time τ, conditioned on the occurrence of an event at time t_0, as

$$F_\tau(x\,|\,t_0) \equiv \Pr\{\tau \leqslant x\,|\,\text{event at time } t_0\} \tag{A3}$$

and the density of counts $p_N(n, x\,|\,t_0)$ in the interval $(t_0, t_0 + x]$ as

$$p_N(n, x\,|\,t_0) \equiv \Pr\{\text{number of events } N \text{ in } (t_0, t_0 + x] = n\} \tag{A4}$$

$F_\tau(x|t_0)$ is related to the distribution of counts $p_N(n, x|t_0)$ by

$$F_\tau(x\,|\,t_0) = 1 - p_N(n, x\,|\,t_0)|_{n=0} \tag{A5}$$

$p_N(0, x\,|\,t_0)$ depends solely on the integrated rate $M_x(t_0)$ (Saleh 1978)

$$p_N(0, x\,|\,t_0) = \exp[-M_x(t_0)] \tag{A6}$$

so that

$$F_\tau(x\,|\,t_0) = 1 - \exp[-M_x(t_0)] \tag{A7}$$

Since we are considering the integrated rate $M_x(t_0)$ between events, we can include the effects of dead time by a simple modification to (1), namely,

$$M_x(t_0) = \int_{t_0+\tau_d}^{t_0+x} \lambda(y)\,\mathrm{d}y \tag{A8}$$

The conditional probability density function $p_\tau(x\,|\,t_0)$ is then

$$p_\tau(x\,|\,t_0) = \frac{\partial F_\tau(x\,|\,t_0)}{\partial x} = \exp[-M_x(t_0)]\frac{\partial M_x(t_0)}{\partial x} \tag{A9}$$

Since the rate is a monotonic, deterministic function of time, conditioning on t_0 is equivalent to conditioning on λ_0, with $\lambda_0 = \lambda(t_0)$. Hence,

$$p_\tau(x\,|\,\lambda_0) = \exp[-M_x(t_0)]\frac{\partial M_x(t_0)}{\partial x} \tag{A10}$$

where, from (A2),

$$t_0 = \tau_1 \ln\left(\frac{\lambda_1}{\lambda_0}\right) \tag{A11}$$

With $\lambda(t)$ approximately constant over the duration of an interval, then (A10), using (4) and (A8), becomes

$$p_\tau(x\,|\,\lambda_0) = \lambda_0 \exp\left(-x\lambda_0 + \frac{1}{k-1}\right) \quad x > \tau_d \tag{A12}$$

To remove the conditioning we exhaustively sample all values attained by $\lambda(t)$ over the duration of the experiment $[t_1, t_1 + L]$ (Teich and Card 1979). The corresponding density function $p_{\lambda 0}(\lambda_0)$ is then.

$$p_{\lambda 0}(\lambda_0) = \frac{\tau_1}{\lambda_0 L} \quad \lambda_{\min} \leqslant \lambda_0 \leqslant \lambda_{\max} \tag{A13}$$

where

$$\lambda_{\max} = \lambda_1 \exp(-t_1/\tau_1)$$

and

$$\lambda_{\min} = \lambda_1 \exp[-(t_1 + L)/\tau_1]$$

Finally, removing the conditioning from (A12) we obtain

$$p_\tau(x) \propto \int_{\lambda_{\min}}^{\lambda_{\max}} \lambda_0 p_\tau(x\,|\,\lambda_0) p_{\lambda 0}(\lambda_0)\,\mathrm{d}\lambda_0 \tag{A14}$$

with the scale factor λ_0 introduced because the number of intervals generated with a particular rate λ is directly proportional to λ. This scale factor is necessary because the distribution corresponds to intervals generated during a single realization of the process. Alternatively, if each of an ensemble of realizations were to be sampled, with the sample time uniformly distributed over the duration of the realization, then the scale factor would not be necessary. In this latter case, however, the effects of length-biased sampling would have to be corrected (Cox and Lewis 1966).

Returning to our formalism, (A14) yields

$$p_\tau(x) = \begin{cases} 0 & x < \tau_{d,\min} \\ \dfrac{c}{x^2}\left\{\dfrac{k}{k-1}\,\mathrm{e}^{\frac{-1}{k-1}} - \mathrm{e}^{-x\lambda_{\max}}(x\lambda_{\max} + 1)\right\} & \tau_{d,\min} \leqslant x \leqslant \tau_{d,\max} \\ \dfrac{c}{x^2}\{\mathrm{e}^{-x\lambda_{\min}}(x\lambda_{\min} + 1) - \mathrm{e}^{-x\lambda_{\max}}(x\lambda_{\max} + 1)\} & x > \tau_{d,\max} \end{cases} \tag{A15}$$

where

$$\tau_{d,\min} = \frac{1}{(k-1)\lambda_{\max}}$$

$$\tau_{d,\max} = \frac{1}{(k-1)\lambda_{\min}}$$

and c is a normalizing constant, implicitly defined by requiring $p_\tau(x)$ to have unity area. This is the final result for the interevent time probability density function.

Analytical results have been obtained (Vannucci and Teich 1978; Prucnal and Teich 1983) for the count distribution, and the mean and variance, of an inhomogeneous DTMP with dead time τ_d, subject to the conditions $\tau_d \ll \tau_c$; $\tau_d \ll T$; and $\{E[\lambda]\tau_d\}^2\tau_d/6 \ll \tau_c$, where τ_c is the characteristic time of the rate function and T is the counting time. The first and last restrictions are satisfied by the parameters shown in Table 1, and our analysis will apply only for counting times sufficiently large such that the second condition is obeyed as well. With an exponential rate

$$\lambda_d(t) = \left(\frac{k-1}{k}\right)\lambda(t) = \left(\frac{k-1}{k}\right)\lambda_1 \exp(-t/\tau_1)$$

[see (A1)] and a counting interval T initiated at t_0, where t_0 is a random time uniformly distributed over the duration of the experiment $[t_1, t_1 + L]$, we obtain (Prucnal and Teich 1983, Table 1)

$$E\{N\} = \frac{\tau_1^2\lambda_d(t_1)}{L}(1 - e^{-T/\tau_1})(1 - e^{-L/\tau_1}) \tag{A16}$$

$$\mathrm{Var}\{N\} = E\{N\}\left\{\left(\frac{k-1}{k}\right)^2 + \frac{\lambda_d(t_1)\tau_1^2}{2L}(1 - e^{-T/\tau_1}) \times\left[\left(\frac{L}{\tau_1} - 2\right) + \left(\frac{L}{\tau_1} + 2\right)e^{-L/\tau_1}\right]\right\} \tag{A17}$$

This provides the analytical result for the Fano factor, which is simply the ratio of the count variance to mean, subject to the condition $T \gg \tau_d$.

The results developed above can be used in the derivation of an analytical expression for the SCC:

$$\mathrm{SCC}(T) = \frac{\mathrm{Cov}(N_1, N_2)}{[\mathrm{Var}(N_1)\mathrm{Var}(N_2)]^{1/2}} = \frac{E\{N_1N_2\} - E\{N_1\}E\{N_2\}}{[\mathrm{Var}(N_1)\mathrm{Var}(N_2)]^{1/2}} \tag{A18}$$

with N_1 the number of counts in $(t_0, t_0 + T]$, and N_2 the number of counts in $(t_0 + T, t_0 + 2T]$, where t_0 is a random variable uniformly distributed over the duration of the experiment, $[t_1, t_1 + L]$. Expressing the expectation of N_1N_2 as

$$E\{N_1N_2\} = E\{E(N_1N_2|t_0)\} \tag{A19}$$

N_1 and N_2, conditioned on t_0, can be treated as independent if the effects of dead time are neglected. After some calculation we obtain

$$\mathrm{SCC}(T) = \frac{\left\{\frac{\tau_1\lambda_d(t_1)}{2}(1 - e^{-T/\tau_1})(1 + e^{-L/\tau_1}) - E[N_1]\right\}e^{-T/2\tau_1}}{\left\{\left(\frac{k-1}{k}\right)^2 + f\right\}^{1/2}\left\{\left(\frac{k-1}{k}\right)^2 + fe^{-T/\tau_1}\right\}^{1/2}} \tag{A20}$$

where

$$f = \frac{\lambda_d(t_1)\tau_1^2}{2L}(1 - e^{-T/\tau_1})\left\{\left(\frac{L}{\tau} - 2\right) + \left(\frac{L}{\tau} + 2\right)e^{-L/\tau_1}\right\}$$

The SCC analytical result accounts for the correlation introduced by the time-varying rate, but it neglects the (negative) correlation imposed by dead time.

References

Cant N, Casseday J (1986) Projections from the anteroventral cochlear nucleus to the lateral and medial superior olivary nuclei. J Comp Neurol 247:457–476

Cox DR, Lewis PAW (1966) The statistical analysis of series of events. Chapman and Hall, London

Guinan J, Norris B, Guinan S (1972) Single auditory units in the superior olivary complex. II Locations of unit categories and tonotopic organization. Int J Neurosci 4:147–166

Johnson DH, Swami A (1983) The transmission of signals by auditory-nerve fiber discharge patterns. J Acoust Soc Am 74:493–501

Johnson DH, Tsuchitani C, Linebarger DA, Johnson MJ (1986) Application of a point process model to responses of cat lateral superior olive units to ipsilateral tones. Hearing Res 21:135–159

Lowen SB, Teich MC (1991) Doubly stochastic Poisson point process driven by fractal shot noise. Phys Rev A 43:4192–4215

Prucnal PR, Teich MC (1979) Statistical properties of counting distributions for intensity-modulated sources. J Opt Soc Am 69:539–544

Prucnal PR, Teich MC (1983) Refractory effects in neural counting processes with exponentially decaying rates. IEEE Trans Syst Man Cybern 13:1028–1033

Saleh B (1978) Photoelectron statistics. Springer, New York

Saleh B, Teich MC (1982) Multiplied-Poisson noise in pulse, particle and photon detection. Proc IEEE 70:229–245

Teich MC (1985) Normalizing transformations for dead-time-modified Poisson counting distributions. Biol Cybern 53:121–124

Teich MC (1989) Fractal character of the auditory neural spike train. IEEE Trans Biomed Eng 36:150–160

Teich MC (1992) Fractal neuronal firing patterns. In: McKenna T, Davis J, Zornetzer S (eds) Single neuron computation. Academic, Boston, pp 589–625

Teich MC, Diament P (1969) Flat counting distribution for triangularly-modulated Poisson process. Phys Lett 30A:93–94

Teich MC, Diament P (1980) Relative refractoriness in visual information processing. Biol Cybern 38:187–191

Teich MC, Khanna SM (1985) Pulse-number distribution for the neural spike train in the cat's auditory nerve. J Acoust Soc Am 77:1110–1128

Teich MC, Matin L, Cantor BI (1978) Refractoriness in the maintained discharge of the cat's retinal ganglion cell. J Opt Soc Am 63:386–402

Teich MC, Johnson DH, Kumar AR, Turcott RG (1990a) Rate fluctuations and fractional power-law noise recorded from cells in the lower auditory pathway of the cat. Hearing Res 46:41–52

Teich MC, Turcott RG, Lowen SB (1990b) The fractal doubly stochastic Poisson point process as a model for the cochlear neural spike train. In: Dallos P, Geisler CD, Matthews, JW, Ruggero MA, Steele CR (eds) The mechanics and biophysics of hearing. Springer, New York, pp 354–361

Tsuchitani C (1982) Discharge patterns of cat lateral superior olivary units to ipsilateral tone-burst stimuli. J Neurophysiol 47:479–500

Tsuchitani C (1988) The inhibition of cat lateral superior olivary unit excitatory responses to binaural tone bursts. II. The sustained discharges. J Neurophysiol 59:184–211

Tsuchitani C, Boudreau JC (1966) Single unit analysis of cat superior olive *S*-segment with tonal stimuli. J Neurophysiol 28:684–697

Tsuchitani C, Johnson DH (1985) The effects of ipsilateral tone burst stimulus level on the discharge patterns of cat lateral superior olivary units. J Acoust Soc Am 77:1484–1496

Vannucci G, Teich MC (1978) Effects of rate variation on the counting statistics of dead-time-modified Poisson processes. Opt Commun 25:267–272

Young ED, Barta PE (1986) Rate responses of auditory nerve fibers to tones in noise near masked threshold. J Acoust Soc Am 79:426–442

Zacksenhouse M, Johnson DH, Tsuchitani C (1992) Excitatory/inhibitory interaction in the LSO revealed by point process modeling. Hearing Res 62:105–123

Zook J, DiCaprio R (1988) Intracellular labeling of afferents to the lateral superior olive in the bat. Hearing Res 34:141–148